Supporting Information

Topotactic Phase Transformation of Lithiated Spinel to Layered $LiMn_{0.5}Ni_{0.5}O_2$: The Interaction of 3-D and 2-D Li-ion Diffusion

Boyu Shi[1], Jihyeon Gim[1], Tianyi Li[2], Krishna Koirala[3], Chongmin Wang[4], Dewen Hou[5,6], Yuzi Liu[5], Jacob Jorne[7], Jason R. Croy[1], Michael M. Thackeray[1], and Eungje Lee[1,*]

[1] Electrochemical Energy Storage Department, Chemical Sciences and Engineering Division, Argonne National Laboratory, Lemont, IL 60439, USA

[2] X-ray Science Division, Advanced Photon Source, Argonne National Laboratory, Lemont, IL 60439, USA

[3] Physical and Computational Sciences Directorate, Pacific Northwest National Laboratory, Richland, WA 99354, USA

[4] Environmental Molecular Sciences Laboratory, Pacific Northwest National Laboratory, Richland, WA 99354, USA

[5] Nanoscience and Technology Division, Argonne National Laboratory, Lemont, IL 60439, USA

[6] Micron School of Materials Science and Engineering, Boise State University, Boise, Idaho 83725, USA

[7] Department of Chemical Engineering, University of Rochester, Rochester, NY 14627, USA

Table S1. The 1st cycle charge/discharge specific capacity and the initial Coulombic efficiency of Li/LMNO400-900 cells (V = 2.5-5.0 V vs. Li, *i* = 15 mA/g, 30 °C).

Sample	1st cycle charge capacity (mAh/g)	1st cycle 1st discharge capacity (mAh/g)	Initial Coulombic efficiency
LMNO400	268.4	223.0	83.0%
LMNO500	238.7	196.2	82.2%
LMNO600	211.4	179.7	85.0%
LMNO700	201.6	174.7	86.7%
LMNO800	207.6	187.4	90.3%
LMNO900	224.4	188.9	84.2%

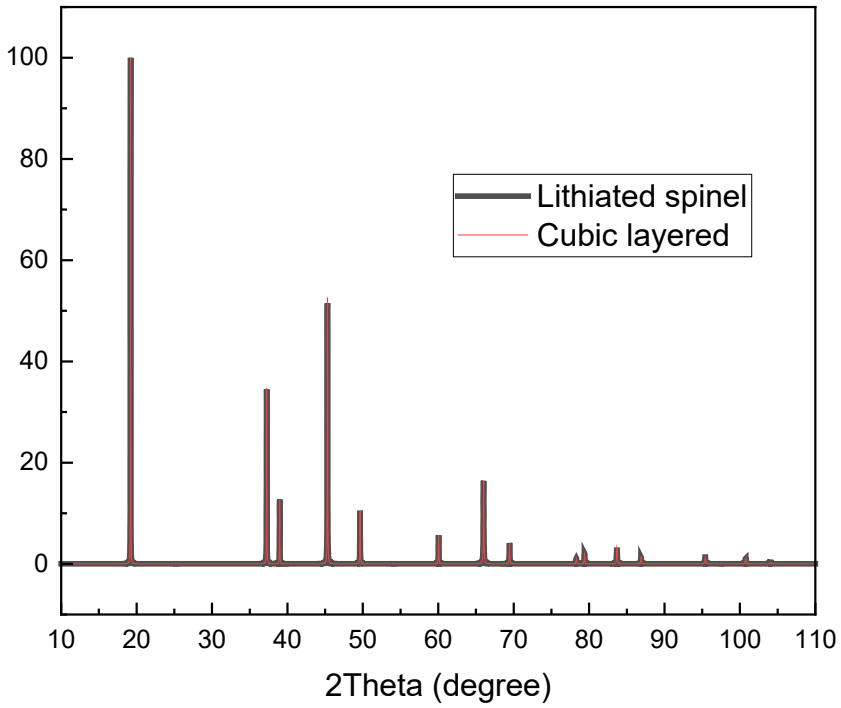

Figure S1. Calculated XRD patterns for a cubic (*Fd*-3*m*) lithiated spinel $LiMO_2$ ($Li_2M_2O_4$) structure and a trigonal (*R*-3*m*) layered $LiMO_2$ structure such as $LiCoO_2$ ($Li_2Co_2O_4$) that are identical, as described in [E. Rossen, J. N. Reimers, and J. R. Dahn, Synthesis and Electrochemistry of Spinel LT-$LiCoO_2$. *Solid State Ionics*, 1993, **62**, 53-60].

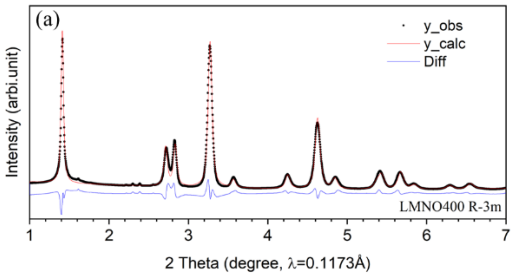

a=2.901035 Å, c=14.22494 Å, c/a=4.903; R_{wp}=13.783, Kai^2= 17.22

Atom	Position	x	y	z	Occ	U
Li1	3a	0	0	0	0.822	0.0406
Li2	3b	0	0	0.5	0.178	0.0018
M1	3a	0	0	0	0.178	0.0406
M2	3b	0	0	0.5	0.822	0.0018
O	6c	0	0	0.238	1	0.0109

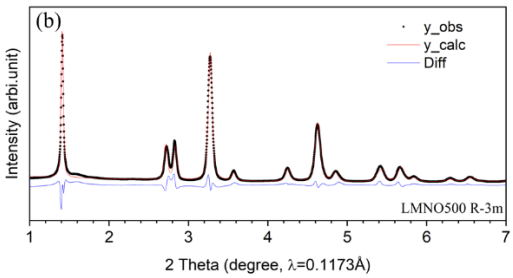

a=2.89817 Å, c=14.23131 Å, c/a=4.91; R_{wp}=12.036, Kai^2= 9.25

Atom	Position	x	y	z	Occ	U
Li1	3a	0	0	0	0.840	0.041
Li2	3b	0	0	0.5	0.160	0.0015
M1	3a	0	0	0	0.160	0.041
M2	3b	0	0	0.5	0.840	0.0015
O	6c	0	0	0.242	1	0.0104

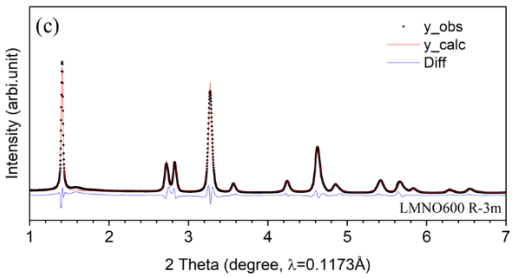

a=2.89483 Å, c=14.28206 Å, c/a=4.934; R_{wp}=11.107, Kai^2= 8.61

Atom	Position	x	y	z	Occ	U
Li1	3a	0	0	0	0.864	0.041
Li2	3b	0	0	0.5	0.136	0.0015
M1	3a	0	0	0	0.136	0.041
M2	3b	0	0	0.5	0.864	0.0015
O	6c	0	0	0.243	1	0.0104

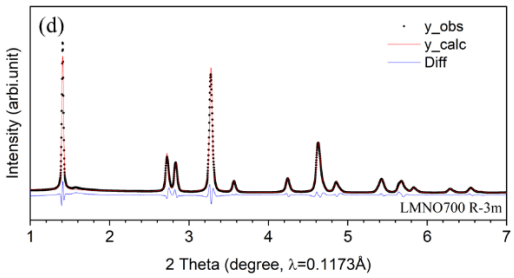

a=2.89322 Å, c=14.28879 Å, c/a=4.939; R_{wp}=10.296, Kai^2= 7.82

Atom	Position	x	y	z	Occ	U
Li1	3a	0	0	0	0.877	0.021
Li2	3b	0	0	0.5	0.123	0.0088
M1	3a	0	0	0	0.123	0.021
M2	3b	0	0	0.5	0.877	0.0088
O	6c	0	0	0.259	1	0.0096

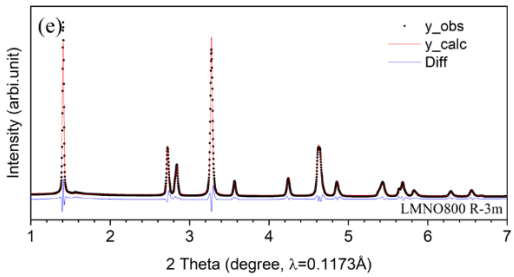

a=2.89222 Å, c=14.29834 Å, c/a=4.944; R_{wp}=8.565, Kai^2= 6.68

Atom	Position	x	y	z	Occ	U
Li1	3a	0	0	0	0.893	0.021
Li2	3b	0	0	0.5	0.107	0.0088
M1	3a	0	0	0	0.107	0.021
M2	3b	0	0	0.5	0.893	0.0088
O	6c	0	0	0.258	1	0.0096

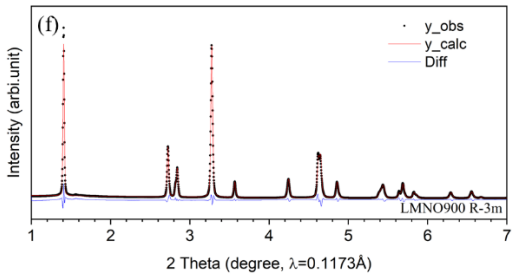

a=2.889658 Å, c=14.29168 Å, c/a=4.945; R_{wp}=8.424, Kai^2= 6.37

Atom	Position	x	y	z	Occ	U
Li1	3a	0	0	0	0.899	0.0017
Li2	3b	0	0	0.5	0.101	0.0063
M1	3a	0	0	0	0.101	0.0017
M2	3b	0	0	0.5	0.899	0.0063
O	6c	0	0	0.258	1	0.0092

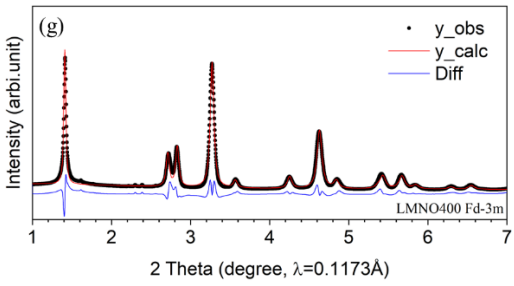

a=8.20883 Å; R_{wp}=11.808, Kai^2= 14.75

Atom	Position	X	y	z	Occ	U
Li1	16c	0	0	0	0.817	0.0125
Li2	16d	0.5	0.5	0.5	0.183	0.0062
M1	16c	0	0	0	0.183	0.0125
M2	16d	0.5	0.5	0.5	0.817	0.0062
O	32e	0	0	0.257	1	0.0201

Figure S2. XRD Rietveld refinement data of (a-f) LMNO400-900 with *R*-3*m* symmetry and (g) LMNO400 sample with *Fd*-3*m* symmetry.

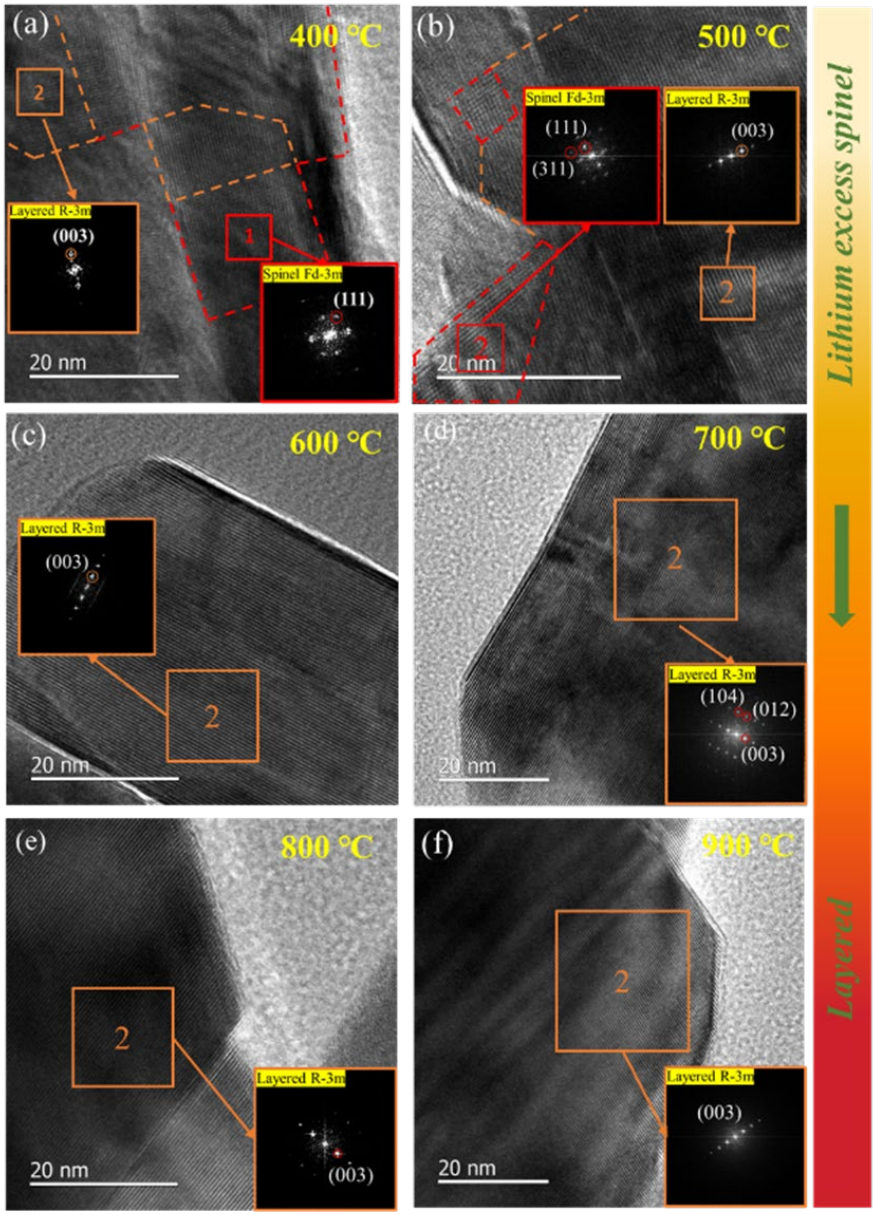

Figure S3. HR-TEM images and FFTs (inset) of (a) LMNO400, (b) LMNO500, (c) LMNO600, (d) LMNO700, (e) LMNO800, and (d) LMNO900.

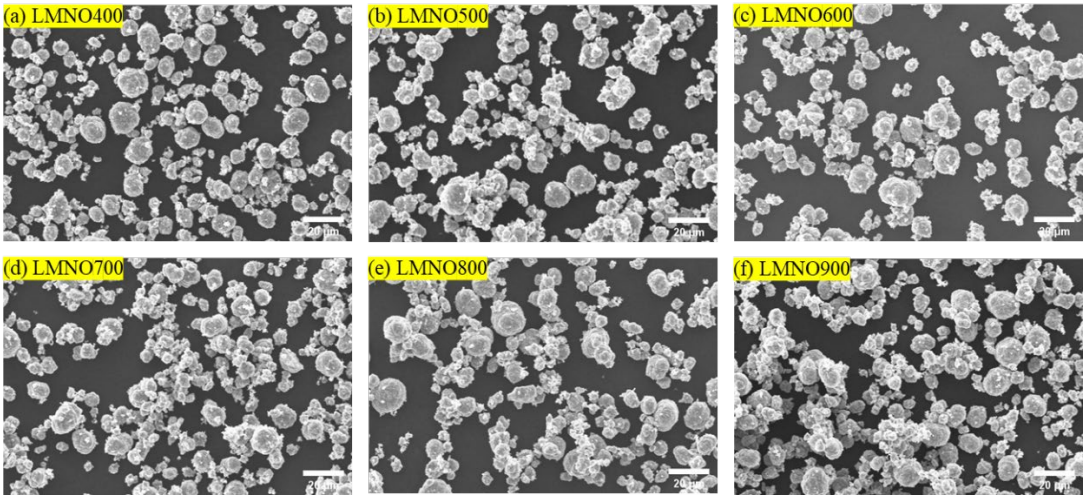

Figure S4. SEM images of (a) LMNO400, (b) LMNO500, (c) LMNO600, (d) LMNO700, (e) LMNO800, and (f) LMNO900 samples.

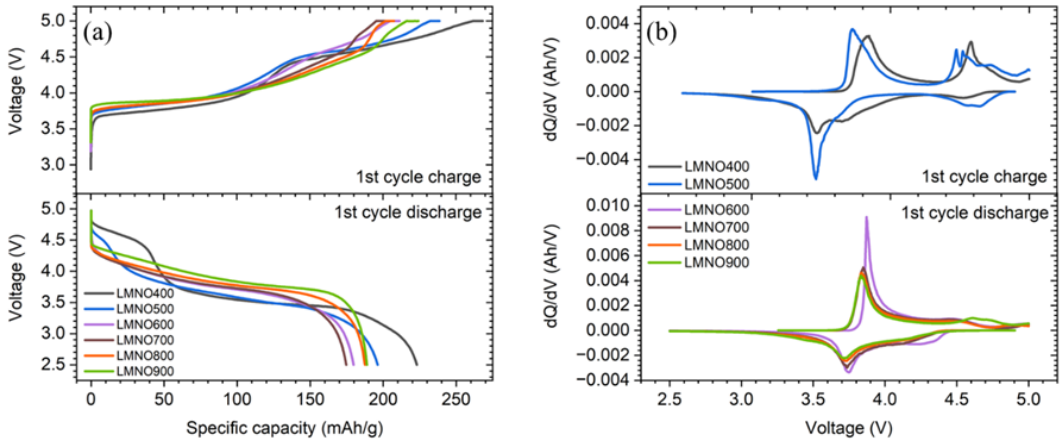

Figure S5. (a) The 1st charge-discharge voltage profiles and (b) dQ/dV plots of Li/LMNO400-900 cells (V = 2.5-5.0 V vs. Li, *i* = 15 mA/g, 30 °C).

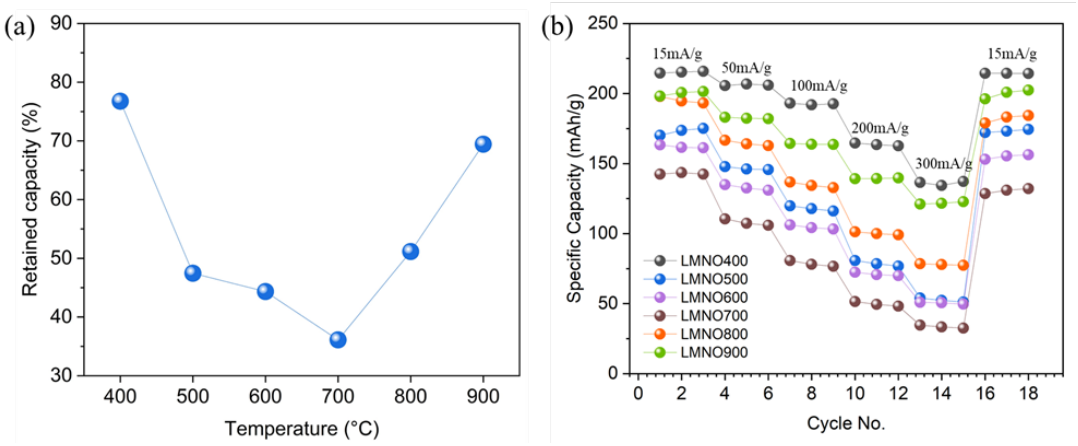

Figure S6. (a) LMNO400-900 electrodes' percentage of retained capacity at 200 mA/g with respect to 15 mA/g and (b) rate performance for the LMNO400-900 electrodes (V = 2.5-5.0 V vs. Li, 30 °C).

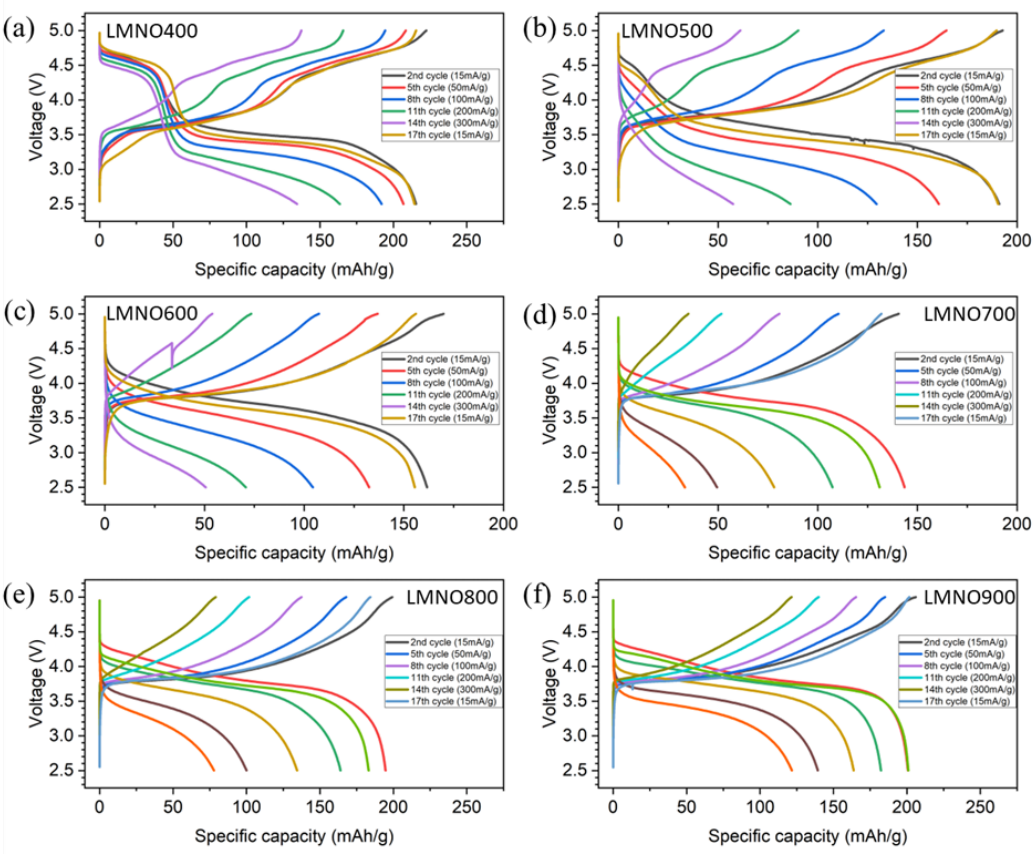

Figure S7. Representative voltage profiles of the (a)-(f) LMNO400-900 electrodes under different current densities.

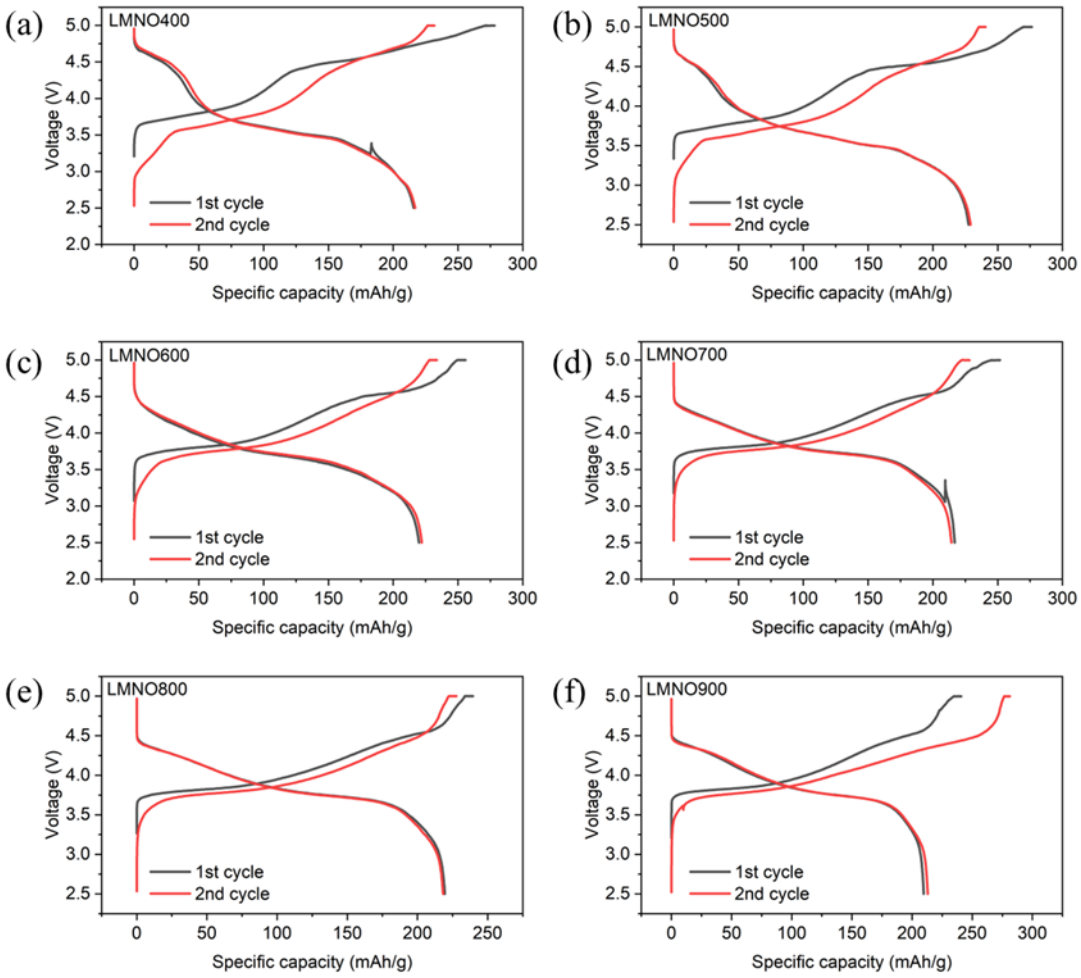

Figure S8. The 1st and 2nd cycle charge-discharge voltage profiles of Li/LMNO400-900 cells tested at 50 ºC (V = 2.5-5.0 V vs. Li, *i* = 15 mA/g).

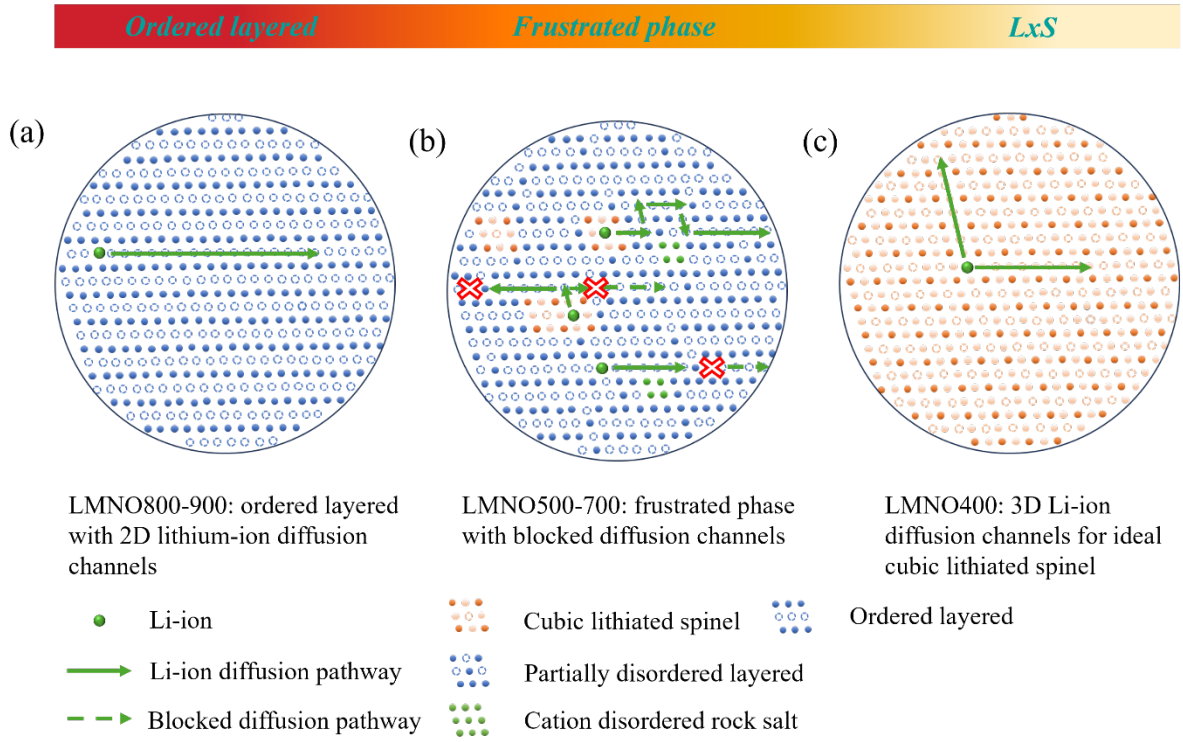

Figure S9. Schematic illustration of the effect of LMNO local structures on Li-ion diffusion channels; (a) ordered layered (b) frustrated structure and (c) LxS.